THE JOURNAL OF PHYSICAL CHEMISTRY Letters

Letter

pubs.acs.org/JPCL

Optical Imaging and Absolute Absorption Cross Section Measurement of Individual Nano-objects on Opaque Substrates: Single-Wall Carbon Nanotubes on Silicon

D. Christofilos,[†] J.-C. Blancon,[‡] J. Arvanitidis,[§] A. San Miguel,[‡] A. Ayari,[‡] N. Del Fatti,*[,⊥] and F. Vallée[⊥]

[†]Physics Division, School of Technology and [§]Physics Department, Aristotle University of Thessaloniki, 54124 Thessaloniki, Greece
[‡]LPMCN and [⊥]LASIM — FemtoNanoOptics, Université Lyon 1, CNRS, 43 Bd du 11 Novembre, 69622 Villeurbanne, France

Supporting Information

ABSTRACT: Optical detection of an individual single nano-object on an opaque substrate and direct determination of its absorption cross section is demonstrated using reflective spatial modulation spectroscopy. This method is applied to optical imaging and investigation of individual single-wall carbon nanotubes in the 1.6 nm diameter range on silicon substrates, which are also individually characterized by atomic force microscopy, scanning electron microscopy, and in situ micro-Raman spectroscopy. Absorption cross sections on the order of 10^{-17} cm^2 per carbon atom are measured for the investigated semiconducting carbon nanotubes, with a light polarization absorption anisotropy of about 2.

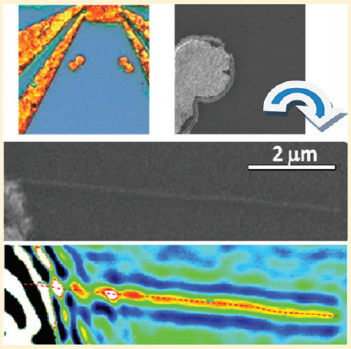

SECTION: Plasmonics, Optical Materials, and Hard Matter

Optical methods are powerful noncontact and nondestructive probes of matter. In nanosciences, optical detection and imaging combined with spectroscopic investigations yield crucial information on optical, structural, electronic, or mechanical properties of nano-objects and nanomaterials. Their extension to single nano-objects constitutes an important advance, avoiding the inherent averaging effects of ensemble studies and thus permitting detailed investigation of nano-objects' properties as a function of their morphology and environment.[1] For nonluminescent single nano-objects, optical detection and spectroscopy methods are based on observation of either their light scattering or absorption.[2−7] Though they have now been used to investigate many different nanosystems, for example, individual carbon nanotubes (CNTs) or metal nanoparticles, their application down to few-nanometer sizes requires nano-objects deposited on transparent substrates or suspended in order to minimize the background signal.[2−10] This strongly limits their applicability, excluding investigation of many nanostructures and nanodevices fabricated on opaque or strongly absorbing substrates like carbon or silicon, widely used in fabrication procedures and technological applications. It also puts many constraints on their combination with other characterization tools requiring specific substrates, as for transmission electron microscopy.

We demonstrate here that this limitation can be overcome by removing the optical contribution of the substrate using a local differential technique, reflective spatial modulation spectroscopy (RSMS). Its principle of operation is analogous to transmission spatial modulation spectroscopy (SMS) used to investigate single nanoparticles on transparent substrates[5,11−13] and later applied to suspended CNTs.[14] It is based on spatially moving the nano-object in and out of the focal spot of a tightly focused light beam and measuring the resulting modulation of its reflection. The amplitude of the reflectivity modulation is directly related to the extinction cross section of the nano-object, permitting its direct determination at the illuminating wavelength λ. We used this method to optically image individual single-wall carbon nanotubes (SWCNTs) grown on silicon substrates and to perform the first direct measurement of their absorption cross section. The same nanotubes were individually investigated by atomic force microscopy, scanning electron microscopy, and in situ micro-Raman spectroscopy, permitting comparison with the obtained optical images and identification of the investigated SWCNTs.

The carbon nanotubes were synthesized by chemical vapor deposition (CVD) on a commercial degenerated silicon substrate with a 300 nm thick SiO_2 layer. Iron nanoparticles were deposited by dipping the substrate first into a solution of $Fe(NO_3)_3$ in isopropanol and then into hexane. Nanotubes were then grown in a tube furnace at 900 °C for 10 min using a mixture of H_2, CH_4, and C_2H_4. Alignment markers were fabricated before the nanotube growing by optical lithography, evaporation of 20 nm of Cr and 250 nm of gold, and lift off.

Received: March 23, 2012
Accepted: April 19, 2012

   dx.doi.org/10.1021/jz300361g | J. Phys. Chem. Lett. 2012, 3, 1176−1181

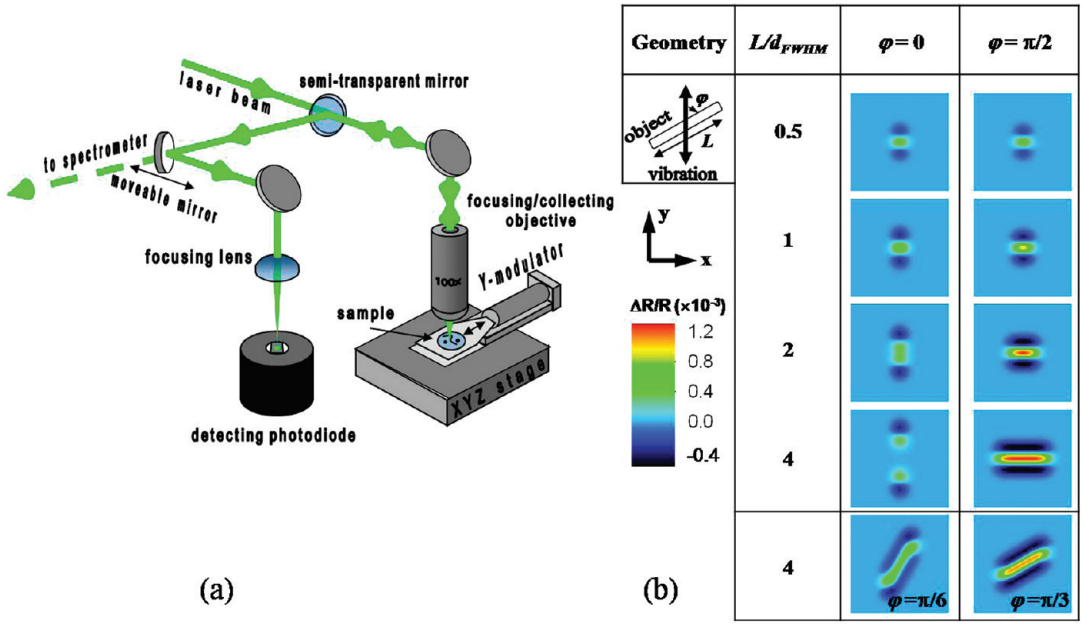

Figure 1. Optical setup for combined RSMS and Raman measurements and simulated RSMS images of an absorbing nano-object. (a) Schematic of the combined RSMS/Raman spectroscopy system. (b) Computed RSMS images of a cylinder of diameter much smaller than its length, L, for different ratios of its length to the focal spot size (L/d_{fwhm}) and different angles φ of the cylinder axis direction relative to the modulation direction y. The size of each image is 4 d_{fwhm} × 4 d_{fwhm}. The $\Delta R/R$ amplitudes correspond to an absorption cross section of σ_{abs} = 0.3 nm^2/nm, d_{fwhm} = 400 nm, and full modulation amplitude $2\Delta y_0$ = 540 nm.

Samples were imaged with a FEI NOVA NANOSEM 450 FEG scanning electron microscope and a Veeco Nanoscope IIIa atomic force microscope in tapping mode. Samples with low surface density of CNTs were prepared so that they could be easily optically separated, taking into account the limited spatial resolution of the far-field optical method (on the order of the full width at half-maximum, d_{fwhm}, of the focused laser beam).

Optical detection of individual CNTs was performed by developing a reflective version of the SMS method (Figure 1a). It is based on tightly focusing a laser beam (of incident power P_i) on the surface of a substrate on which nanoparticles with extinction cross section σ_{ext} are deposited. In the presence of a nanoparticle at point (x_0,y_0) in the focal plane, the reflected field is the sum of the one reflected by the substrate and the one scattered by the object.[4,15] Assuming that the particle is much smaller than the focal spot size d_{fwhm} and a small reflectivity R, the reflected power is $P_R \approx RP_i - \sigma_{ext} R^{1/2} I(x_0,y_0)$, where $I(x,y)$ is the incident light beam intensity profile at the focal plane. In the case of layered substrates, as the silicon substrates used for growing the SWCNTs, this expression has to be generalized to take into account Fabry–Perot effects (i.e., the effective field that excites the nano-object at the surface and the reflected field phase). However, the above simple form is valid for real reflection coefficients, and thus, it can still be used for wavelengths close to the Fabry–Perot maxima (around 580 nm for the used substrates. In this case, $R^{1/2}$ has to be replaced by $R^{1/2}$ $F^{1/2}$, where F represents the intensity enhancement factor at the surface due to Fabry–Perot effects). These approximations are fulfilled in our experimental conditions, with, for instance, $R \approx 0.11$ ($F \approx 1.6$) at 561 nm and $R \approx 0.13$ ($F \approx 1.4$) at 633 nm. Displacement by Δy_0 of the nano-object position leads to a change of the reflected power $\Delta P_R \approx -\sigma_{ext} R^{1/2}\{I(x_0,y_{0+}\Delta y_0) - I(x_0,y_0)\}$ (assuming a homogeneous substrate over Δy_0). Harmonic modulation of the particle position (along the y axis) at a frequency f leads to modulation of the relative reflectivity, $\Delta R/R = \Delta P_R/P_R$. Synchronous detection at f or $2f$ of the reflected power change thus permits detection of the presence of a nano-object and quantitative determination of its extinction cross section as this sets the ΔR amplitude. As in SMS,[11] localization of the object is better achieved through signal demodulation at $2f$. When scanning the sample position in the focal plane, a nanoparticle then shows up as a main central peak with two smaller-amplitude minima of opposite sign in the modulation direction (i.e., resembles the second spatial derivative relative to y of the intensity profile $I(x,y)$; see Figure 1b).

In the case of one-dimensional (1D) elongated nano-objects such as carbon nanotubes (with one dimension larger than d_{fwhm} and the others much smaller), similar modeling of the RSMS signals can be performed using the extinction coefficient per unit length $\tilde{\sigma}_{ext}$. For small absorbing nano-objects such as SWCNTs, scattering is negligible as compared to absorption, $\tilde{\sigma}_{sca} \ll \tilde{\sigma}_{abs}$, so that $\tilde{\sigma}_{abs}$ and $\tilde{\sigma}_{ext}$ can be identified ($\tilde{\sigma}_{sca}$ is at least two orders of magnitude smaller than $\tilde{\sigma}_{abs}$ for the investigated SWCNT[10,16]). The absorbed power is then obtained by integrating over the probed nano-object zone, $\int_L \tilde{\sigma}_{abs} I(x,y)\, ds$, where s is the curvilinear abscissa along the 1D object and L is its length. The RSMS signal can then be numerically simulated, as illustrated in Figure 1b, for different object lengths and orientations relative to d_{fwhm} and the modulation direction, y, respectively. For a modulation direction perpendicular to its long axis ($\varphi = \pi/2$ in Figure 1b), the object can be imaged when L is larger than the optical resolution (i.e., d_{fwhm}), yielding the possibility to extract information on its morphology and, importantly, to measure its absorption cross section per unit length $\tilde{\sigma}_{abs}$. Conversely, weaker signals showing only the edges of the object are obtained when y is along its long axis (i.e., φ = 0 in Figure 1b).

The RSMS setup is built around a commercial micro-Raman spectrometer (Figure 1a). This configuration permits straight-

dx.doi.org/10.1021/jz300361g | J. Phys. Chem. Lett. 2012, 3, 1176–1181

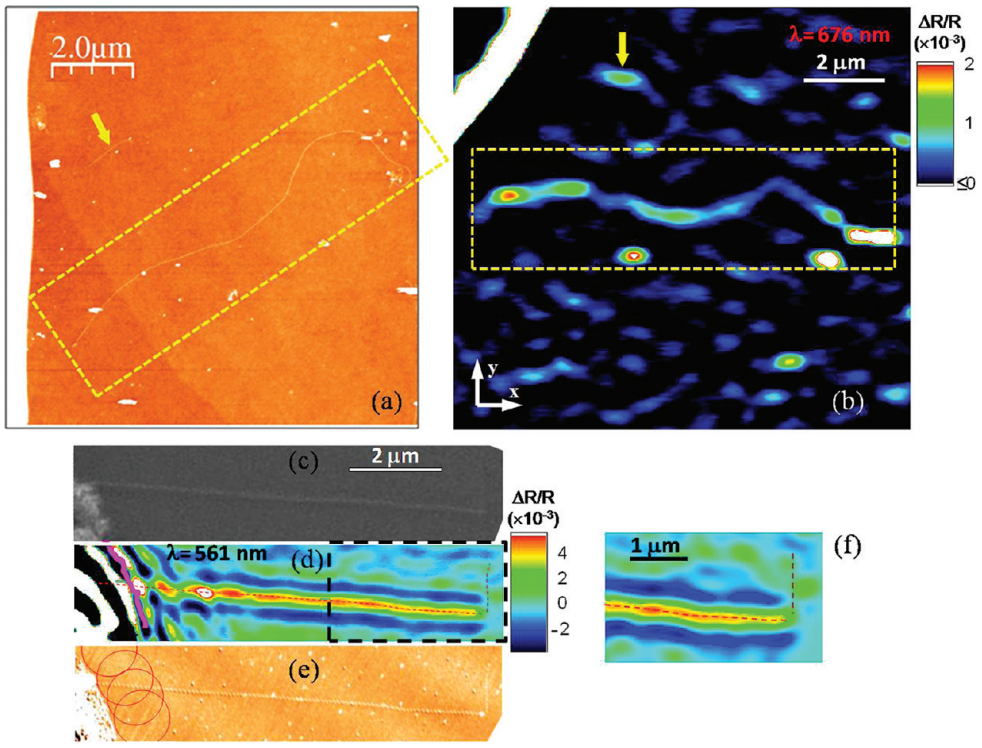

Figure 2. Comparison of the RSMS imaging with other imaging techniques for different individual CNTs on a SiO_2/Si substrate. Upper panel: (a) AFM and (b) RSMS (measured with λ = 676 nm, $d_{fwhm} \approx$ 480 nm, $2\Delta y_0$ = 540 nm along y, and x-polarized light) images of a long (dashed rectangle) and a short (arrow) CNT. Lower panel: (c) SEM, (d) RSMS (with λ = 561 nm, $d_{fwhm} \approx$ 400 nm, $2\Delta y_0$ = 540 nm along y, and x-polarized light), and (e) AFM images of a third CNT close to a lithographically produced contact. The nanotube appears shorter in RSMS than that in AFM or SEM micrographs because of the large contribution of the contact to the optical signal due to the smaller optical resolution consequence of the spot size and sample modulation (circles on the AFM image indicate approximately the zone where the contact influences the RSMS signal; its edge is superimposed on the RSMS image of the nanotube, thick purple line). The RSMS image is in very good agreement with numerical simulations (f) performed on the area depicted by the dashed rectangle in (d). The small vertical nanotube and background particles visible in the AFM image are also taken into account in the simulation.

forward combination with Raman spectroscopy, performed using either the 561 nm line of an Excelsior Newport diode-pumped solid-state laser, the 632.8 nm line of a Melles Griot He−Ne laser, or the 676.4 nm line of a Kr^+ Stabilite 2017 Spectra Physics laser. The sample is fixed on a linear piezoactuator, providing spatial modulation of its position in the y direction at frequency f. The optimal full modulation amplitude, $2\Delta y_0$, is close to d_{fwhm}. An $x-y$ nanopositioning stage allows rastering of the sample on which light is focused and collected by a 100× microscope objective. The reflected light is detected by means of a standard silicon photodiode. As compared to other approaches, this technique directly measures the absorption cross section. The signal $\Delta R/R$ is thus independent of the incident power P_i, and very low intensities are required. This permits the use of low power sources and renders this technique suitable for materials sensitive to photodamage. Typical incident power values are on the order of a few microwatts (corresponding to $I \approx 1$ kW/cm^2), and detected AC voltage levels are in the range of microvolts. Modulating at $f \approx 1.5$ kHz, minimum reflection changes of $(\Delta R/R)_{min} \approx 10^{-5}$ can be detected, corresponding to a sensitivity of a few nm^2 for the nano-object absorption cross section. Similarly to SMS measurements in transmission, sensitivity is mainly limited by the stability of the laser and the mechanical stability of the setup.

RSMS optical images of individual single-wall CNTs grown on SiO_2/Si substrates and their comparison to AFM and/or SEM images are shown in Figure 2. The top AFM and RSMS images show the same two individual CNTs, a long and a short one, indicated by the dashed frame and the arrow, respectively. Their diameter estimated from the AFM image is about 1.6 nm. For both CNTs, modulation in RSMS measurement was performed perpendicular to their mean direction (Figure 2b). Several catalytic and/or "debris" nanoparticles of the production process are also visible with always very good one-to-one correspondence between the AFM and RSMS images (as $2f$ detection is used here, a nano-object should appear as a main peak with two negative satellites in RSMS images; the latter have been suppressed to enhance image readability by appropriately setting the black level of the false-color scale). The RSMS signal profile along the tube axis is the spatial convolution of the laser spot and the nanotube shape, while it reflects the laser beam intensity profile along the perpendicular direction, in agreement with our simulations (Figure 1b). The short CNT thus shows up as a weakly elongated object in the optical image as its length, of about 1 μm, is comparable to the beam diameter d_{fwhm} (≈0.5 μm for the used wavelength, λ = 676 nm). In contrast, the morphology of the long CNT is very well observed, with the transverse RSMS spatial signal being still determined by the laser intensity profile. Bright spots along the CNT are mainly due to the catalyst particles, while fluctuations of the contrast can be attributed to variations of the CNT direction as compared to the modulation direction and to possible changes of the nanotube characteristics along its length.[17] The CNTs are observed for all of the different wavelengths used in this study, with wavelength-

dx.doi.org/10.1021/jz300361g | J. Phys. Chem. Lett. 2012, 3, 1176−1181

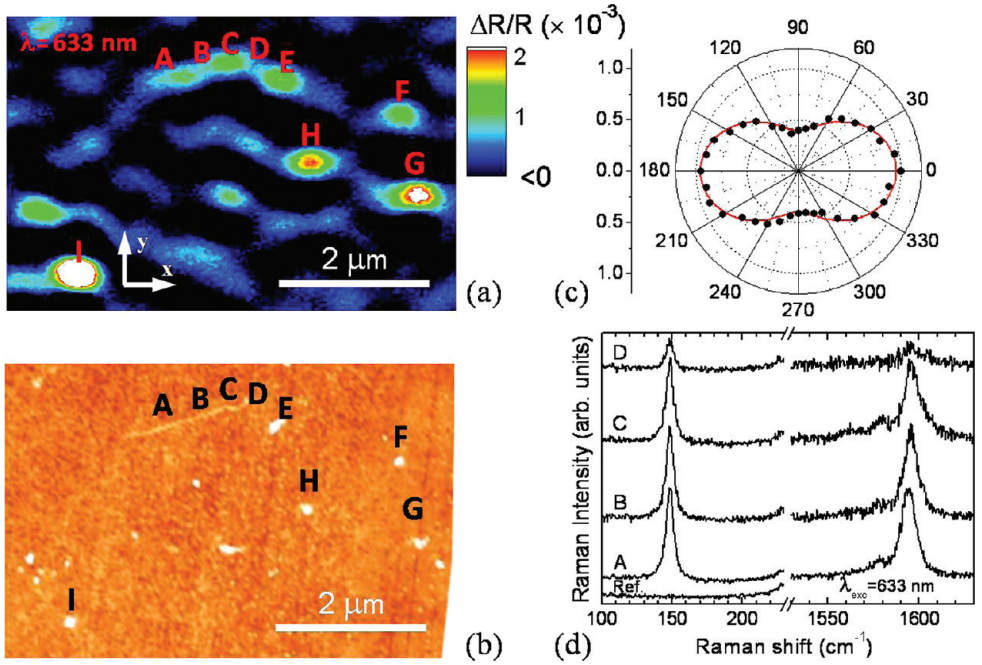

Figure 3. Combination of RSMS and Raman spectroscopy. (a) RSMS (with λ = 633 nm, $d_{fwhm} \approx$ 450 nm, $2\Delta y_0$ = 540 nm along y, and x-polarized light) and (b) AFM images of a CNT on a SiO_2/Si substrate. (c) Light-polarization-dependent RSMS signal recorded from point B on the nanotube. The same dependence is obtained for different points A–D on the CNT, while the RSMS signals of the dusts or debris, points E–I, show no light polarization dependence. (d) Raman spectra acquired at selected spots (A–D on the RSMS image) showing the CNT radial breathing mode (RBM) at 148 cm^{-1} and its G-band peak (tangential modes) around 1595 cm^{-1}. The laser at λ = 633 nm is polarized along the x-direction with an incident power of 1 mW. A reference spectrum from an "empty" area of the sample is also shown. Raman spectra from spots E–I of the RSMS image resemble the reference spectrum (not shown).

dependent signal amplitudes. This wavelength-independent detection stresses the high potentiality of the technique for high-contrast optical imaging and detection of individual CNTs via their absorption (see also the Supporting Information for further details).

The impact of the modulation direction relative to the nano-object orientation is illustrated in the lower panel of Figure 2, showing the SEM, RSMS, and AFM images of the same CNT in contact with a metallic electrode used as a marker (Figure 2c–e, respectively). A full RSMS image is shown using a false-color scale, the CNT appearing as a main positive peak with two negative satellites along the modulation direction almost perpendicular to its axis (Figure 2d). The different images are well-correlated, except for the short nanotube almost perpendicular to the main one that is visible in AFM and SEM. As this CNT is almost parallel to the modulation direction, it only yields a weak RSMS signal. This is confirmed by the excellent agreement of the RSMS with the simulated image, obtained using the measured AFM shape as an input (Figure 2f; the fine nanoparticles observed in the AFM micrographs were also taken into account). Note that acquisition of RSMS images for two orthogonal modulation directions would avoid this orientation-dependent effect and permit detection of all of the individual nanotubes present on the substrate.

Though determination of the absorption cross section of the detected SWCNT can be straightforwardly performed from the RSMS signal, it is of interest only if the specific CNT is identified. In this direction, Raman spectroscopy has been employed as the wealth of information obtained from the CNT Raman spectra make it a powerful technique for their characterization and identification.[18] In combined RSMS and Raman studies, the CNT is first detected optically using RSMS, its Raman spectrum being subsequently measured in situ with the same setup. This is illustrated in Figure 3, showing the RSMS image and the Raman spectrum of a short CNT of ~2 μm length, in the region between A and D. Both were measured using a He–Ne laser at λ = 633 nm linearly polarized along x (as expected, no significant Raman signal was observed for a polarization perpendicular to the nanotube axis[19]). Excellent agreement between the RSMS image and the AFM one was again obtained, showing in particular the same additional catalyst particles (some of them are indicated as the E–I points in Figure 3a and b). Several Raman spectra have been acquired in all letter-specified spots. Characteristic CNT spectra were apparent only at the A–D spots, showing both the CNT radial breathing modes (RBM) and the G-band peaks (Figure 3d). The frequency of the former is inversely proportional to the nanotube diameter d_t, which, in our systems, can be estimated using the expression established for vertically aligned SWCNTs synthesized by CVD on a quartz substrate, $\omega_{RBM}(cm^{-1}) = 217.8/d_t + 15.7$ (with d_t in nanometers).[20] The measured RBM frequency ($\omega_{RBM} \approx$ 148 cm^{-1}) yields $d_t \approx$ 1.65 nm for the investigated CNT, in agreement with the value range of 1.5–1.7 nm estimated by AFM. The RBM Raman line is observed for λ = 633 nm excitation but not for the other wavelengths used (i.e., 561 and 676 nm). Using a recent Kataura plot,[20] this suggests a close-to-resonance excitation condition with the E_{33} transition of the (18,5) semiconducting SWCNT.

Following the identification of the SWCNT, its absorption cross section per unit length $\tilde{\sigma}_{abs}(\lambda)$ can be determined from the measured RSMS signal amplitude, $\Delta R/R$, using the model presented in Figure 1b. Its resonant absorption cross section

dx.doi.org/10.1021/jz300361g | J. Phys. Chem. Lett. 2012, 3, 1176–1181

(i.e., at around 633 nm where the RBM Raman line is observed) for light polarized along its axis is estimated to be $\tilde{\sigma}_{abs}$ (633 nm) ≈ 0.35 nm^2/nm (corresponding to about 1.8×10^{-17} cm^2/carbon atom). As expected, the values obtained for the out-of-resonance conditions are smaller, yielding $\tilde{\sigma}_{abs}$ (56lnm) $\approx 0.6 \times 10^{-17}$ cm^2/carbon atom. These directly measured cross section values around the E_{33} transition of a semiconducting SWCNT are consistent with those indirectly deduced in recent experiments for the E_{11} and E_{22} transitions of single-wall CNTs in transparent environments.[10,21,22] The polarization dependence of σ_{abs} can also be straightforwardly determined (Figure 3c). It exhibits a contrast factor of about 2.3:1 for light polarization parallel or orthogonal to the CNT axis, respectively. Similar polarization anisotropy has been obtained for different CNTs at wavelengths in and out of resonance with one of their electronic transitions (with a mean contrast of about 2:1). Our direct measurement is in very good agreement with the polarization absorption anisotropy determined indirectly in recent photoinduced current experiments in individual CNTs.[23] Conversely, Rayleigh and Raman scattering studies show much larger contrast associated with a stronger antenna effect,[8,16,19] emphasizing the different nature of the involved light−matter interaction mechanisms.

In summary, we have demonstrated a new far-field optical technique, reflective spatial modulation spectroscopy (RSMS), enabling optical imaging and quantitative investigation of single absorbing nano-objects on opaque substrates. On the basis of an extension of the spatial-modulation technique, in the reflection geometry, it permits high-contrast optical imaging of single nano-objects on strongly absorbing substrates. Demonstrated for individual SWCNTs on silicon, optical images were found to be in excellent agreement with AFM and SEM micrographs, providing a new method for optical detection of individual CNTs. Using this method, the absolute value and light polarization dependence of the absorption cross section of a CNT were directly determined for the first time, yielding values on the order of 10^{-17} cm^2 per carbon atom (around the E_{33} transition of a semiconducting SWCNT of about 1.6 nm diameter). Our studies can be straightforwardly extended to determination of the full wavelength dependence (using a tunable laser source) of the absorption of a single CNT. As compared to other techniques, RSMS has the advantages of being quantitative, easily implementable, and appropriate for very low power measurements. More generally, it opens the way to optical investigation of a broad range of nanomaterials and devices fabricated on nontransparent substrates. Furthermore, the flexibility and ease of integration of this method makes it easily combinable with other optical (Raman) or nonoptical (AFM or electron microscopy) nanoscale characterization tools without strong requirements on the used substrate.

■ ASSOCIATED CONTENT

Supporting Information

Additional information includes RSMS images for different CNTs, illuminating wavelengths, and light polarization, with corresponding Raman spectra. This material is available free of charge via the Internet at http://pubs.acs.org.

■ AUTHOR INFORMATION

Corresponding Author

*E-mail: delfatti@lasim.univ-lyon1.fr.

Notes

The authors declare no competing financial interest.

■ ACKNOWLEDGMENTS

The authors thank CNRS for support through the PICS Program Number 4917. N.D.F. also acknowledges the support of Institut Universitaire de France.

■ REFERENCES

(1) Biswas, A.; Wang, T.; Biris, A. S. Single Metal Nanoparticle Spectroscopy: Optical Characterization of Individual Nanosystems for Biomedical Applications. *Nanoscale* **2010**, *2*, 1560−1572.

(2) Mock, J. J.; Barbic, M.; Smith, D. R.; Schultz, D. A.; Schultz, S. Shape Effects in Plasmon Resonance of Individual Colloidal Silver Nanoparticles. *J. Chem. Phys.* **2002**, *116*, 6755−6759.

(3) Sonnichsen, C.; Franzl, T.; Wilk, T.; von Plessen, G.; Feldmann, J. Plasmon Resonances in Large Noble-metal Clusters. *New J. Phys.* **2002**, *4*, 93.

(4) Lindfors, K.; Kalkbrenner, T.; Stoller, P.; Sandoghdar, V. Detection and Spectroscopy of Gold Nanoparticles Using Supercontinuum White Light Confocal Microscopy. *Phys. Rev. Lett.* **2004**, *93*, 037401.

(5) Arbouet, A.; Christofilos, D.; Del Fatti, N.; Vallée, F.; Huntzinger, J. R.; Arnaud, L.; Billaud, P.; Broyer, M. Direct Measurement of the Single-Metal-Cluster Optical Absorption. *Phys. Rev. Lett.* **2004**, *93*, 127401.

(6) Berciaud, S.; Cognet, L.; Blab, G. A.; Lounis, B. Photothermal Heterodyne Imaging of Individual Nonfluorescent Nanoclusters and Nanocrystals. *Phys. Rev. Lett.* **2004**, *93*, 257402.

(7) Gaiduk, A.; Yorulmaz, M.; Ruijgrok, P. V.; Orrit, M. Room-Temperature Detection of a Single Molecule's Absorption by Photothermal Contrast. *Science* **2010**, *330*, 353−356.

(8) Sfeir, M. Y.; Wang, F.; Huang, L.; Chuang, C.-C.; Hone, J.; O'Brien, S. P.; Heinz, T. F.; Brus, L. E. Probing Electronic Transitions in Individual Carbon Nanotubes by Rayleigh Scattering. *Science* **2004**, *306*, 1540−1543.

(9) Berciaud, S.; Cognet, L.; Poulin, Ph.; Weisman, R. B.; Lounis, B. Absorption Spectroscopy of Individual Single-Walled Carbon Nanotubes. *Nano Lett.* **2007**, *7*, 1203−1207.

(10) Joh, D. Y.; Kinder, J.; Herman, L. H.; Ju, S. Y.; Segal, M. A.; Johnson, J. N.; Chan, G. K. L.; Park, J. Single-walled Carbon Nanotubes as Excitonic Optical Wires. *Nat. Nanotechnol.* **2011**, *4*, 51−56.

(11) Muskens, O. L.; Billaud, P.; Broyer, M.; Del Fatti, N.; Vallee, F. Optical Extinction Spectrum of a Single Metal Nanoparticle: Quantitative Characterization of a Particle and of Its Local Environment. *Phys. Rev. B* **2008**, *78*, 205410.

(12) Muskens, O. L.; Bachelier, G.; Del Fatti, N.; Vallee, F.; Brioude, A.; Jiang, X. C.; Pileni, M. P. Quantitative Absorption Spectroscopy of a Single Gold Nanorods. *J. Phys. Chem. C* **2008**, *112*, 8917−8921.

(13) Baida, H.; Billaud, P.; Marhaba, S.; Christofilos, D.; Cottancin, E.; Crut, A.; Lerme, J.; Maioli, P.; Pellarin, M.; Broyer, M.; et al. Quantitative Determination of the Size Dependence of Surface Plasmon Resonance Damping in Single Ag@SiO(2) Nanoparticles. *Nano Lett.* **2009**, *9*, 3463.

(14) Wang, F.; Cho, D. J.; Kessler, B.; Deslippe, J.; Schuck, P. J.; Louie, S. G.; Zettl, A.; Heinz, T. F.; Shen, Y. R. Observation of Excitons in One-Dimensional Metallic Single-Walled Carbon Nanotubes. *Phys. Rev. Lett.* **2007**, *99*, 227401.

(15) Bohren, C. F.; Huffman, D. R. *Absorption and Scattering of Light by Small Particles*; John Wiley & Sons: New York,1998.

(16) Heinz, T. F. Rayleigh Scattering Spectroscopy. In *Carbon Nanotubes*; Topics in Applied Physics; Jorio, A.; Dresselhaus, G.; Dresselhaus, M. S.Eds.; Springer-Verlag: New York, 2008, Vol. *111*, pp 353−369.

(17) Joh, D. Y.; Herman, L. H.; Ju, S. Y.; Kinder, J.; Segal, M. A.; Johnson, J. N.; Chan, G. K. L.; Park, J. On-Chip Rayleigh Imaging and Spectroscopy of Carbon Nanotubes. *Nano Lett.* **2011**, *11*, 1−7.

(18) Dresselhaus, M. S.; Dresselhaus, G.; Saito, R.; Jorio, A. Raman Spectroscopy of Carbon Nanotubes. *Phys. Rep.* **2005**, *409*, 47−99.
(19) Duesberg, G. S.; Loa, I.; Burghard, M.; Syassen, K.; Roth, S. Polarized Raman Spectroscopy on Isolated Single-Wall Carbon Nanotubes. *Phys. Rev. Lett.* **2000**, *85*, 5436−5439.
(20) Araujo, P. T.; Doorn, S. K.; Kilina, S.; Tretiak, S.; Einarsson, E.; Maruyama, S.; Chacham, H.; Pimenta, M. A.; Jorio, A. Third and Fourth Optical Transitions in Semiconducting Carbon Nanotubes. *Phys. Rev. Lett.* **2007**, *98*, 067401.
(21) Berciaud, S.; Cognet, L.; Lounis, B. Luminescence Decay and the Absorption Cross Section of Individual Single-Walled Carbon Nanotubes. *Phys. Rev. Lett.* **2008**, *101*, 077402.
(22) Schoeppler, F.; Mann, Ch.; Hain, T. C.; Neubauer, F. M.; Privitera, G.; Bonaccorso, F.; Chu, D.; Ferrari, A. C.; Hertel, T. Molar Extinction Coefficient of Single-Wall Carbon Nanotubes. *J. Phys. Chem. C* **2011**, *115*, 14682−14686.
(23) Tsen, A. W.; Donev, L. A. K.; Kurt, H.; Herman, L. H.; Park, J. Imaging the Electrical Conductance of Individual Carbon Nanotubes with Photothermal Current Microscopy. *Nat. Nanotechnol.* **2009**, *4*, 108−113.